Earth and Planetary Science Letters 317-318 (2012) 396–406

Contents lists available at SciVerse ScienceDirect

Earth and Planetary Science Letters

journal homepage: www.elsevier.com/locate/epsl

How large is the subducted water flux? New constraints on mantle regassing rates

R. Parai *, S. Mukhopadhyay

Department of Earth and Planetary Sciences, Harvard University, 20 Oxford Street, Cambridge, MA 02138, United States

ARTICLE INFO

Article history:
Accepted 21 November 2011
Available online xxxx

Editor: R.W. Carlson

Keywords:
water
subduction
noble gases
post-arc flux
long-term sea level
serpentinite

ABSTRACT

Estimates of the subducted water (H_2O) flux have been used to discuss the regassing of the mantle over Earth history. However, these estimates vary widely, and some are large enough to have reduced the volume of water in the global ocean by a factor of two over the Phanerozoic. In light of uncertainties in the hydration state of subducting slabs, magma production rates and mantle source water contents, we use a Monte Carlo simulation to set limits on long-term global water cycling and the return flux of water to the deep Earth. Estimates of magma production rates and water contents in primary magmas generated at ocean islands, mid-ocean ridges, arcs and back-arcs are paired with estimates of water entering trenches via subducting oceanic slab in order to construct a model of the deep Earth water cycle. The simulation is constrained by reconstructions of Phanerozoic sea level change, which suggest that ocean volume is near steady-state, though a sea level decrease of up to 360 m may be supported. We provide limits on the return flux of water to the deep Earth over the Phanerozoic corresponding to a near steady-state exosphere (0–100 meter sea level decrease) and a maximum sea level decrease of 360 m. For the near steady-state exosphere, the return flux is $1.4-2.0^{+0.4}_{-0.3}\times10^{13}$ mol/yr, corresponding to 2–3% serpentinization in 10 km of lithospheric mantle. The return flux that generates the maximum sea level decrease over the Phanerozoic is $3.5^{+0.4}_{-0.3}\times10^{13}$ mol/yr, corresponding to 5% serpentinization in 10 km of lithospheric mantle. Our estimates of the return flux of water to the mantle are up to 7 times lower than previously suggested. The imbalance between our estimates of the return flux and mantle output flux leads to a low rate of increase in bulk mantle water content of up to 24 ppm/Ga.

1. Introduction

Exchange of water between the Earth's interior and the exosphere (defined here as the atmosphere, ocean and crust) is critically dependent on water systematics at subduction zones. Water is outgassed from the mantle in association with volcanism at mid-ocean ridges, ocean islands, arcs and back-arc basins. Water is removed from the exosphere at subduction zones, carried as pore water and chemically-bound water in sediments, altered oceanic crust and serpentinized lithospheric mantle within the downgoing slab. At a given subduction zone, some amount of subducted water is released from the slab due to breakdown of hydrous minerals at high pressure and temperature; this slab-derived water flux drives melting in the mantle wedge and is ultimately outgassed to the exosphere via arc and back-arc volcanism. Any water retained within the subducting slab beyond depths of magma generation constitutes a return flux of water to the interior, often referred to as the post-arc subducted water flux (Fig. 1). A quantitative assessment of the long-term water cycle is critical to our understanding of a wide variety of solid Earth phenomena: the abundance and distribution of water in the Earth's interior have dramatic effects on mantle melting (e.g. Hirschmann, 2006; Inoue, 1994), rheology (e.g. Hirth and Kohlstedt, 1996; Karato and Jung, 2003; Mei and Kohlstedt, 2000), structure and style of convection (Crowley et al., 2011), and a return flux of exospheric water to the deep interior may affect cycling of other volatiles, such as the noble gases (Holland and Ballentine, 2006). Here we present new constraints on water exchange between the mantle and exosphere over the past 542 Ma.

Previous estimates of the deep Earth water return flux are based on calculations of the equilibrium stability of hydrous phases at subduction zone pressures and temperatures (e.g., Hacker, 2008; Rüpke et al., 2004; Schmidt and Poli, 1998, 2003; van Keken et al., 2011). Assuming an initial slab lithology and estimated pressure–temperature (P–T) conditions for a particular subduction zone, the water content of the equilibrium phase assemblage is determined as a function of depth. Thus, the amount of water retained in the slab past depths of magma generation is estimated by tracking the breakdown of hydrous phases along a given P–T path of subduction. However, in order to obtain an estimate of the global return flux of water to the deep Earth, initial slab lithologies and P–T profiles at individual subduction zones around the world must be established (Hacker, 2008; van Keken et al., 2011). Thus, such estimates of the deep Earth water return flux are subject to significant uncertainty, particularly with respect to the serpentinite content of the lithospheric mantle. While serpentinized lithospheric mantle could be generated by

* Corresponding author.
E-mail address: parai@fas.harvard.edu (R. Parai).

0012-821X/$ – see front matter © 2011 Elsevier B.V. All rights reserved.
doi:10.1016/j.epsl.2011.11.024

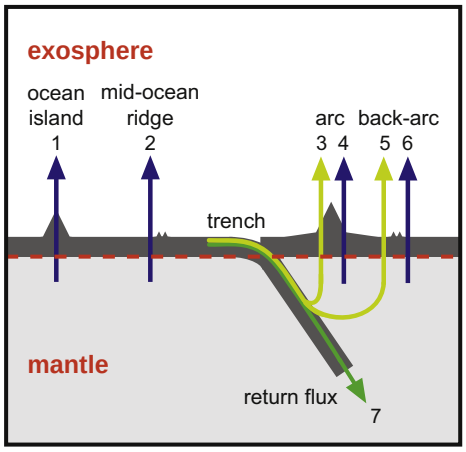

Fig. 1. Schematic of global water fluxes considered between the mantle and exosphere. Water is outgassed from the mantle due to magmatism at ocean islands, mid-ocean ridges, arcs and back-arcs (arrows 1–6). Water is removed from the exosphere at trenches. Some fraction of the trench input flux is directly outgassed via the arc and back-arc system (arrows 3 and 5). The majority of arc and back-arc water output is thought to be slab-derived, but some portion is derived from water present in the ambient mantle wedge (arrows 4 and 6). Water retained past depths of magma generation constitutes a return flux of water to the deep Earth (arrow 7). The net flux between mantle and exosphere is determined by the difference between the return flux and mantle-derived output fluxes.

seawater infiltration along transform faults or deep faults (15–20 km) into the oceanic plate at the outer rise (Nedimovic et al., 2009; Ranero et al., 2003, 2005), the degree and spatial extent of serpentinization around the faults remain poorly constrained.

Reasonable physical considerations can be used to establish upper limit or order-of-magnitude constraints on the amount of water carried by serpentinized lithosphere in the subducting slab. Schmidt and Poli (1998) use buoyancy considerations to set an upper limit on the extent of lithospheric serpentinization: since serpentinite is less dense than unaltered peridotite, serpentinization lessens the negative buoyancy of the subducting slab. A 10 km thick section of lithosphere with average 10% serpentinization has a density of 3.15 g/cm^3 (Schmidt and Poli, 1998); beyond this degree of serpentinization, slab descent becomes problematic. Alternately, Li and Lee (2006) use an approximation of the spatial distribution of faults and fractures in oceanic lithosphere and an estimated lateral extent of serpentinization around faults or fractures (based on the diffusivity of water in serpentinite) to compute an order-of-magnitude estimate of initial slab hydration condition. However, order-of-magnitude estimates may represent the difference between removing an ocean's worth of water from the exosphere in 5 Ga vs. 500 Ma.

We take an alternative approach to assess long-term cycling of water between the exosphere and the mantle. We use independent constraints on (a) mantle water output fluxes and (b) global sea level change over time to provide limits on the initial slab water input flux, as well as the return flux of water to the deep mantle. A statistical (Monte Carlo) approach is used to efficiently search the parameter space (which is based on literature estimates of water input at subduction zones and output at ocean islands, mid-ocean ridges, arcs and back-arcs) for water cycling scenarios that best satisfy constraints on Phanerozoic sea level change. We do not track the breakdown of hydrous phases or make assumptions regarding whether the water return flux circulates within the upper mantle or is injected into the lower mantle. Rather, we focus on establishing limits on the magnitudes of global fluxes across the mantle–exosphere boundary to provide key constraints on the following questions:

(1) How much water is subducted into the mantle at trenches?
(2) What fraction of the water subducted into the mantle is recycled past the arcs into the deep Earth?

2. Model

Fig. 1 shows the fluxes considered in our model of the global water cycle. Based on literature estimates, we define upper and lower limits for ten model parameters (Table 1). Total magmatic water output fluxes are computed by coupling literature estimates of magma production rate to primary magmatic water contents at each tectonic setting. Input fluxes at trenches are drawn from literature estimates of the amount of chemically-bound water carried in subducting slabs, and a Monte Carlo technique is used to explore the entire parameter space. A successful run meets two criteria: (1) the global slab-derived arc and back-arc water output does not exceed the global water input at trenches; and (2) the imbalance between mantle input and output fluxes is consistent with reconstructions of Phanerozoic sea level change.

2.1. Defining the model parameter space

Mantle output fluxes are quantified based on magma production rates (Table 1) and the range of measured magmatic water contents at individual tectonic settings (Table 1; see the full compilation in Supplementary Table S1). We assume that over the Phanerozoic, secular variation in mid-ocean ridge magma production rates has not exceeded 20% of present day rates (Table 1). There is no evidence for secular change in seafloor spreading rates over the past 180 Ma (Parsons, 1982; Rowley, 2002), and our assumption is further supported by studies indicating limited change in mantle potential temperature of ~50–100 K per Ga (Abbott et al., 1994; Labrosse and Jaupart, 2007; Vlaar et al., 1994), as well as geodynamic models indicating a change in heat flow of only ~10% in the past Ga (van Keken et al., 2001). We double the upper limit OIB magma production rate of Crisp (1984) in order to capture possible elevated long-term mean production rates associated with flood basalt volcanism.

The trench water input flux is carried as pore water and chemically-bound water in sediments, altered oceanic crust and, potentially, serpentinized lithospheric mantle. Pore water is thought to be entirely expelled from the slab at shallow levels and returned to the exosphere (Jarrard, 2003) and so we do not discuss it further. A summary of literature estimates of the chemically-bound water flux into trenches is given in Table 2. We note that most of the flux magnitudes are in broad agreement, with the exception of Schmidt and

Table 1
Model Parameter Space.

Parameter	min	max	References
Magma production rate at:	(km^3/yr)	(km^3/yr)	
Ocean islands	1.8	4.8	Crisp (1984)
Mid-ocean ridges	17	25	Reymer and Schubert (1984)
Arcs	1.1	8.6	Reymer and Schubert (1984); Crisp (1984)
Fraction N-MORB:	0.8	0.9	
Primary magmatic H_2O content[a] in:	(wt.%)	(wt.%)	
Ocean island basalt	0.3	1.6	Simons et al. (2002)
N-MORB	0.04	0.26	Almeev et al. (2008); Pineau et al. (2004)
E-MORB	0.26	0.92	Michael (1995); Standish et al. (2008)
Arc basalt	1.0	6.0	Benjamin et al. (2007); Roggensack (2001)
Back-arc basin basalt	0.1	2.8	Fretzdorff et al. (2002); Newman et al. (2000)
	($\times 10^{13}$ mol/yr)		
Trench input flux:	4.1	16	Jarrard (2003); Schmidt and Poli (1998)

[a] Full compilation of measured magmatic water contents by tectonic setting in supplement: Table S1. The compilation shows that measured values fill in the ranges listed above.

Poli (1998), who estimate an altered igneous crust lower limit flux that by itself exceeds some of the other total bound water flux estimates. The bulk of the Schmidt and Poli (1998) altered igneous flux is carried by 3.5 km of water-saturated basalt, which may be considered as a carrying capacity. Total estimates of the chemically-bound water flux into trenches vary from 4.1 to 16×10^{13} mol/yr.

2.2. Model setup

A single Monte Carlo realization of the global water cycle draws a random value from the allowed range to represent the global mean for each of the ten model parameters: magma production rate at ocean islands, mid-ocean ridges, and arcs; proportion of N-MORB out of total MORB production; primary magmatic water content in ocean island basalt, N-MORB, E-MORB, arc basalt and back-arc basin basalt; and lastly, trench water input flux. Since back-arc spreading occurs at rates comparable to mid-ocean ridge spreading, the back-arc production rate is computed by scaling the selected MORB production rate by the present-day ratio of back-arc to mid-ocean ridge length (~10%, Baker and German, 2004). Mantle water output fluxes are computed by multiplying magmatic water content by magma production rate at each tectonic setting, assuming a density of 2.9 g/cm^3 for OIB, MORB and back-arc production, and 2.8 g/cm^3 for arcs (Plank, 2005). The total water flux into the trench is drawn from literature estimates for initial chemically-bound water content in the subducting slab, and the fraction of trench input flux that is returned to the exosphere is determined from H_2O–Ti systematics in arc and back-arc basalts (Section 2.3.1). Thus, all fluxes across the mantle-exosphere boundary are specified (Fig. 1). The mantle return flux is the difference between the trench input flux and the slab-derived arc and back-arc water fluxes. Finally, the net flux across the mantle-exosphere boundary is defined as the difference between the mantle output flux and return flux.

2.3. Model constraints

For a given Monte Carlo realization to be classified as a success, the two criteria discussed below must be satisfied:

2.3.1. Model success criterion 1: the global slab-derived arc and back-arc water output must not exceed the global water input at trenches

The combined arc and back-arc magmatic water output flux is derived from two sources: slab fluids released by dehydration reactions, and ambient water in the mantle wedge (Fig. 1). For a given realization, the slab-derived fractions of arc and back-arc output fluxes cannot exceed the trench input flux: i.e., water cannot be created at arcs. This first success criterion requires a method to estimate the fraction of arc and back-arc water output that derives from the slab. The fraction of the arc water flux derived from the slab fluid, f_{slab}, is:

$$f_{slab} = \left(1-f_{mantlewedge}\right) = \frac{\left[(H_2O)_{arc}-(H_2O)_{mantlewedge}\right]}{(H_2O)_{arc}} \quad (1)$$

where $f_{mantlewedge}$ is the fraction of arc water derived from the mantle wedge, $(H_2O)_{arc}$ is the primary magmatic water content of arc magmas, and $(H_2O)_{mantlewedge}$ is the amount of water in the arc magma that is derived from the mantle wedge. The expressions for back-arc water are analogous. Given $(H_2O)_{arc}$ or $(H_2O)_{back\text{-}arc}$, if $(H_2O)_{mantlewedge}$ can be determined, then f_{slab} can be calculated.

We use water–titanium (H_2O–Ti) systematics observed in a global compilation of arc and back-arc basalts to calculate $H_2O_{mantlewedge}$ and thereby estimate the slab-derived component of arc and back-arc water output fluxes in the simulation. Ti is a relatively fluid-immobile element and is not expected to migrate with fluids released due to slab dehydration (Kelley et al., 2006, 2010; Ryerson and Watson, 1987). Thus, Ti in arc and back-arc magmas should be derived primarily from the ambient mantle wedge. Previous work has established that magmatic Ti concentrations are controlled by the degree of partial melting (F) and the Ti concentration in the mantle source (Kelley et al., 2006, 2010; Lee et al., 2005; Stolper and Newman, 1994).

Fig. 2 shows primary magmatic H_2O vs. TiO_2 in a global compilation of arc and back-arc data. A broad negative correlation between H_2O and TiO_2 is evident in the global arc and back-arc data set, though least-squares regression yields distinct slopes for the arc data (slope = −0.079, R = 0.77) and back-arc data (slope = −0.29, R = 0.81). At a given magmatic H_2O content, the observed ~15–25% scatter in magmatic TiO_2 content is likely due to variations in source Ti concentration and the potential temperature of the mantle wedge. However, the broad negative trend in the global data set is consistent with the hypothesis that higher H_2O contents lead to a higher degree of the melting and thus a lower magmatic TiO_2 content, supporting the use of Ti as a proxy for the degree of melting at arc and back-arc environments (Kelley et al., 2006, 2010; Lee et al., 2005; Stolper and Newman, 1994).

While in detail, each arc and back-arc environment is likely to have a slightly different relationship between H_2O and TiO_2 contents, we use the broad correlation in the global data set to model the relationship between arc magmatic H_2O content and degree of melting. We note that the mantle wedge beneath arcs may be heterogeneous and/or depleted with respect to average MORB mantle (e.g., Kelley et al., 2010). To model this, the global average mantle wedge source concentrations of H_2O and Ti are allowed to co-vary between 43 and 320 ppm H_2O (such that 10% melting will produce magmatic H_2O contents between the most depleted N-MORB and a slightly-enriched MORB magmatic H_2O content) and 500 and 1200 ppm Ti (Kelley et al., 2006). The fraction of arc (or back-arc) H_2O output derived from the slab is computed for each realization as follows: once the arc primary magmatic H_2O content has been randomly selected, TiO_2 content in the primary magma is calculated using the best fit slopes for arc H_2O vs. TiO_2, and a ±25% random variation is added to the calculated Ti concentration (±20% for the back-arc) to simulate the scatter observed in the global data set (Fig. 2). Mantle wedge H_2O and Ti concentrations are then drawn from the ranges specified above, and using the batch melting equation and D_{Ti} between 0.04 and 0.10 (Kelley et al., 2006 and references therein), we solve for the degree of melting, F. Since we explore a very large parameter space in D_{Ti} and source Ti concentrations, some realizations

Table 2
Trench input fluxes.

Reference	Water flux ($\times10^{13}$ mol/yr) carried in:			
	Sediment	Altered igneous crust	Serpentinized mantle	Total entering trench
Schmidt and Poli (1998)	0.15–0.30	9.2–12	1.6–6.3	11–16[a]
Jarrard (2003)	0.71	3.4	–	4.1
Rüpke et al. (2004)	0.90	2.6	1.4–6.8	4.8–10
Hacker (2008)	0.83	3.4	3.2	7.4
van Keken et al. (2011)	0.39	3.5	1.7	5.6

[a] Schmidt and Poli (1998) model the slab as 200–400 m sediment, 3.5 km of H_2O-saturated basalt, 3.5 km of hydrated gabbro (20–30% hydration by volume) and 5 km of 5–20% serpentinized mantle. Assuming 2.7 km^2 of convergence per year (Hacker, 2008; Rüpke et al., 2004), this corresponds to a total H_2O flux of $12–18\times10^{13}$ mol/yr. However, Schmidt and Poli (1998) report a total flux into trenches at 20 km of $11–16\times10^{13}$ mol/yr, ~10% lower than the numbers discussed above, possibly reflecting shallow dehydration reactions. We use their preferred total input at 20 km to constrain our trench input flux parameter, and scale the fluxes of sediment, altered crust and serpentinite specified above down to reflect the smaller flux in Fig. 4.

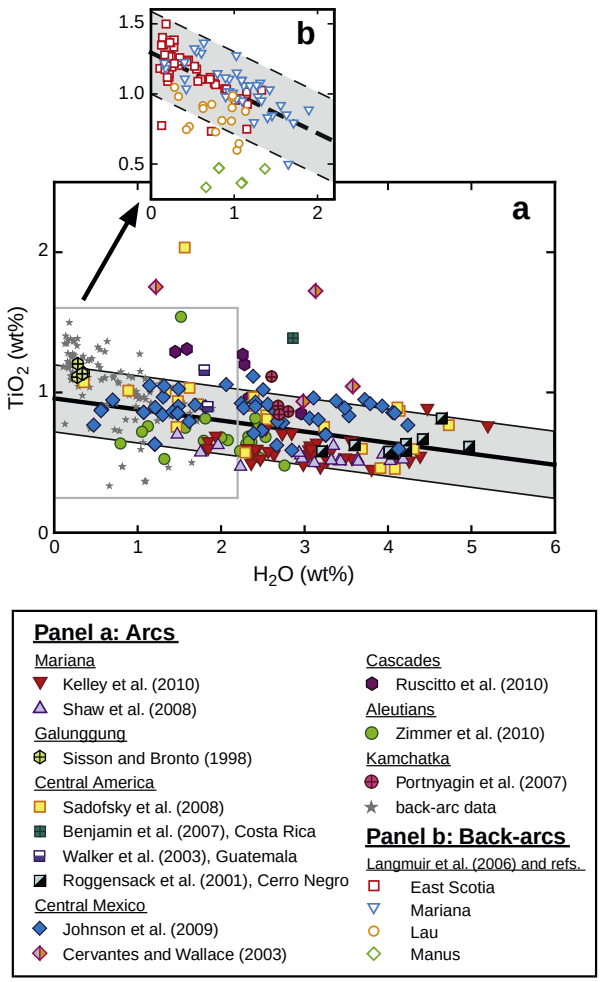

Fig. 2. H_2O–TiO_2 systematics in (panel a) a global compilation of arc melt inclusion data and back-arc glass data. Panel (b) shows the back-arc data in detail (Langmuir et al., 2006, and references therein). Arc melt inclusion data are corrected for fractional crystallization (corrected for post-entrapment crystallization, screened for MgO > 6 wt.%, and brought into equilibrium with Fo_{90} mantle through olivine addition). Back-arc data were compiled and corrected for hydrous fractional crystallization to 8 wt.% MgO by Langmuir et al. (2006). We selected samples with "plagioclase-in" MgO values ≤ 8 wt.% and adjusted the reported $H_{8.0}$ and $Ti_{8.0}$ values of Langmuir et al. (2006) by olivine addition to equilibrium with Fo_{90} mantle (assuming $Fe^{3+}/\Sigma Fe = 0.15$). Least squares regression with bi-square weights to minimize the influence of outliers (robust regression) yields distinct fits for the arc ($y = -0.079x + 0.96$, $R = 0.77$) and back-arc data ($y = -0.29x + 1.29$, $R = 0.81$). There is significant scatter in the global compilation, which probably reflects source Ti heterogeneity as well as variation in subduction zone thermal profiles from arc to arc. We simulate the observed scatter by adding ±25% random variation to the calculated TiO_2 for a given magmatic H_2O content (shaded regions; ±20% for back-arcs). (Data from Benjamin et al., 2007; Cervantes and Wallace, 2003; Johnson et al., 2009; Kelley et al., 2010; Langmuir et al., 2006 and references therein; Portnyagin et al., 2007; Roggensack et al., 2001; Ruscitto et al., 2010; Sadofsky et al., 2008; Shaw et al., 2008; Sisson and Bronto, 1998; Walker et al., 2003; Zimmer et al., 2010).

yield non-physical values of F and are excluded. Non-physical F values indicate that certain combinations of D_{Ti} and source Ti concentration, such as high D_{Ti} and low source Ti concentrations, cannot characterize a real system (also see Kelley et al., 2006).

Once F for a given realization is determined, we use the mantle wedge source H_2O concentration and D_{H2O} between 0.007 and 0.012 (Aubaud et al., 2004; Hauri et al., 2006; Kelley et al., 2006) to calculate the amount of magmatic water derived from the mantle wedge, $(H_2O)_{mantlewedge}$. The fraction of arc water that is derived from the slab is thus determined (Eq. (1)). The same calculation is carried out for back-arcs. The first criterion for success is now tested: if the combined arc and back-arc water demand on the slab exceeds the trench water input flux, then the model realization constitutes a Failure 1 scenario.

2.3.2. Model success criterion 2: net flux must satisfy constraints on Phanerozoic sea level change

We assume that the net flux between the mantle and exosphere is accommodated by the ocean, since it is the dominant exospheric reservoir and hydration of subducting slabs draws water directly from the ocean. Therefore, a long-term sustained imbalance between water supplied to the exosphere by volcanism and water subducted back into the mantle would generate secular global, or eustatic, change in sea level. However, eustatic sea level change may also arise from variation in the volume of the ocean basin, attributed to ~100 Ma-timescale plate tectonic processes such as changes in mid-ocean ridge spreading rates and super-continent cycles (*tectonoeustasy*; e.g. Hays and Pitman, 1973; Schubert and Reymer, 1985), as well as from oscillations in the volume of continental ice sheets on timescales of tens of ka to several Ma (*glacioeustasy*; e.g. Miller et al., 1991, 2005; Zachos et al., 2001). Furthermore, variations in dynamic topography in response to mantle convection may both contribute to ocean basin volume changes, as well as affect local measurements of sea level by vertically displacing the continental platforms on which sediments are deposited (e.g. Conrad and Husson, 2009; Moucha et al., 2008; Muller et al., 2008). Thus, the sedimentary record of long-term sea level reflects a combination of dynamic effects, changes in the volume of the ocean basin, and changes in the volume of water in the oceans.

Continental freeboard studies indicate that sea level has varied by approximately 500 m since the end of the Archean (Galer, 1991; Kasting and Holm, 1992; Windley, 1977; Wise, 1974). However, detailed eustatic sea level reconstructions are only available for the Phanerozoic Eon (e.g., Hallam, 1984, 1992; Haq et al., 1987; Haq and Schutter, 2008; Hardenbol et al., 1981; Vail et al., 1977; Fig. 3). Therefore, we limit our simulation of the water cycle to the Phanerozoic, although we will discuss some implications of our results for water cycling into deep time. The amount of secular eustatic sea level change that may have occurred over the Phanerozoic is estimated by linear regression on the available reconstructions.

Based on the spatial distribution of marine sedimentary facies on continents, Hallam (1984) generates a sea level curve by assuming that present-day continental hypsometry is representative of the entire Phanerozoic. Hallam's sea level curve yields 360 m of secular decrease over 542 Ma (Fig. 3a). Rüpke et al. (2004) adopted ~500 m as the net decrease in Phanerozoic sea level based on Hallam (1984). However, 500 m represents the peak-to-trough variation associated with oscillations in sea level, rather than the magnitude of secular decrease. Furthermore, Algeo and Wilkinson (1991) pointed out that continental hypsometry in the Phanerozoic has not been constant over time, as the continents were widely dispersed during the early Paleozoic. Accordingly, Hallam (1992) reduced the magnitude of the Paleozoic high stand from +600 m to +400 m relative to present-day sea level (Fig. 3b). This modification would reduce the secular trend to yield ~230 m of sea level decrease (Fig. 3b). Therefore, we suggest that Rüpke et al.'s (2004) 500 m overestimates Phanerozoic sea level decrease. While Hallam's reconstruction can support an upper limit of 360 m of sea level decrease (Hallam, 1984), 230 m of secular decrease appears to be more realistic (Hallam, 1992).

Hallam's reconstructions generate the largest secular eustatic sea level decrease out of all available studies. Reconstructions based on seismic reflection data on maritime depositional sequences by Vail et al. (1977), Haq et al. (1987) and Haq and Schutter (2008) show more limited variations (Fig. 3). While Vail et al. (1977) provide only relative eustatic variations in sea level over time (Fig. 3c), Haq et al. (1987) and Haq and Schutter (2008) give absolute variations in sea level with peak-to-trough variations of ~250 m (Fig. 3d). Linear regression yields a secular decrease in sea level equal to 7.8% of the total amplitude for Vail et al. (1977), and a secular *increase* in sea

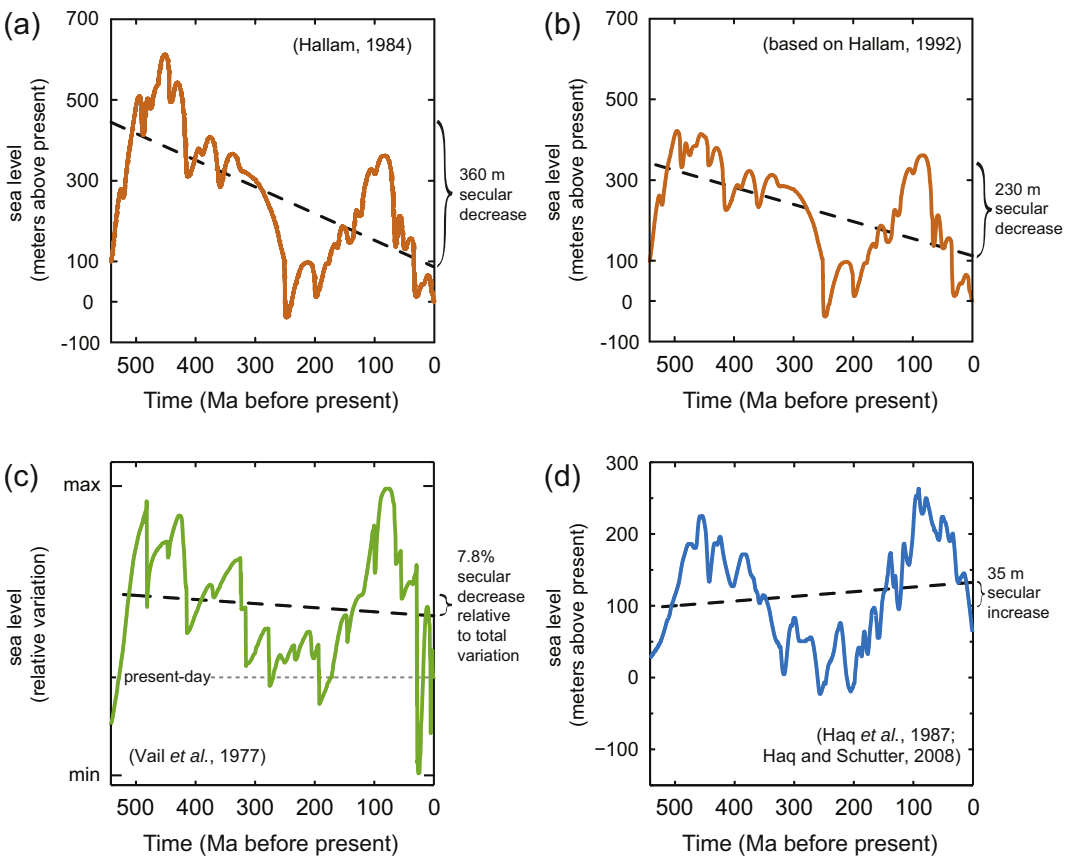

Fig. 3. Reconstructions of Phanerozoic sea level. The magnitude of secular variation that may have occurred is determined by linear regression. (a) Hallam (1984) gives absolute estimates of sea level based on the spatial distribution of marine sedimentary facies on continents, assuming present-day continental hypsometry represents the entire Phanerozoic. Linear regression yields a secular decrease of 360 m over 542 Ma. (b) Hallam (1992) revised his estimated Paleozoic high stand from 600 m to 400 m above present-day, as continental hypsometry likely changed over time and continents were widely dispersed during the early Paleozoic (Algeo and Wilkinson, 1991). We apply a linear scaling to the Paleozoic portion of Hallam's (1984) curve to reflect the revision, and find a decrease in sea level of 230 m over 542 Ma. The ~500 m secular decrease in sea level inferred from Hallam's curve by Rüpke et al. (2004) overestimates the secular change that can be supported by the reconstruction. (c) Vail et al. (1977) give relative estimates of eustatic sea level over the Phanerozoic. Linear regression yields a secular decrease equivalent to 7.8% of the total amplitude. (d) Haq et al. (1987) and Haq and Schutter (2008) give absolute estimates of sea level, yielding a secular *increase* in sea level of 35 m over the Phanerozoic. All reconstructions argue for limited long-term secular variation in sea level.

level of 35 m over the Phanerozoic for Haq et al. (1987) and Haq and Schutter (2008). We note that if the total amplitude of sea level variability is taken as 400 m, then Vail et al. (1977) yields ~30 m of sea level decrease over the Phanerozoic, significantly less than the 230 m estimate based on Hallam (1992).

While the above studies disagree on the precise timing and relative magnitude of specific transgressions and regressions, they share a number of common features. All studies agree in terms of overall shape: sea level rose throughout the Cambrian, broadly fell until ~200 Ma ago, rose and peaked ~100 Ma ago, and then fell to the present day level. The three sea level curves (Fig. 3b–d) all indicate that secular change in sea level, if present, was limited (−230 m for the corrected Hallam curve, −30 m for the Vail curve, and +35 m for the Haq curve, yielding an average of ~−100 m). Hence, we suggest that the sedimentary record is most compatible with a secular decrease of 0–100 m for sea level over the Phanerozoic, which constitutes our preferred scenario ("near steady-state ocean;" Section 4). We cannot rule out a secular increase in long-term sea level from the Phanerozoic record (Fig. 3d); however, since we are interested in setting upper limits on mantle regassing, we will focus on secular sea level decrease. We note that there is no *requirement* for any portion of the observed sea level record to reflect a change in the water budget of the exosphere. For example, previous studies quantitatively ascribe the ~200 m amplitude of sea level change over the past ~60 Ma to changes in ridge volume (Fig. 3; Muller et al., 2008; Xu et al., 2006) dynamic topography (Conrad and Husson, 2009; Moucha et al., 2008) and ice volume (Harrison, 1990). However, if we assume for our simulation that the entire Phanerozoic secular trend reflects the water budget of the exosphere, we can set limits on the imbalance between mantle water input and output fluxes. To an extent, ridge volume and dynamic topography effects may obscure the magnitude, and potentially the sign, of a secular eustatic signal from changes in the exospheric water budget. However, in order to mask a large net inward flux of water into the mantle, ridge volume must increase, or dynamic topography must raise sea level over time. Ridge volume is unlikely to have increased over the Phanerozoic as seafloor spreading rates should generally decrease over long timescales. Furthermore, the age distribution of the ocean floor has either been constant since ~200 Ma (Parsons, 1982; Rowley, 2002) or has increased over the past ~60 Ma (Xu et al., 2006). Dynamic topography is expected to produce sea level changes on order ±100 m in association with a full Wilson cycle (Conrad and Husson, 2009). We therefore use the 360 m decrease of the original Hallam (1984) reconstruction in our model to place an upper limit on the net inward water flux imbalance, despite the fact that it most likely overestimates the magnitude of secular Phanerozoic sea level change. An imbalance between mantle output and input may therefore be tolerated in our model, as long as the net inward flux does not exceed 2.1×10^{13} mol/yr, which is the flux required to reduce sea level by 360 m over 542 Ma (using present-day hypsometry; after Harrison, 1990). We also set a net outward flux limit at 1.9×10^{12} mol/yr, corresponding to a sea level increase of 35 m (Fig. 3d). The second criterion for success can now be assessed: if the net flux is outside the sea level limits, then the realization is classified as a Failure 2 scenario.

Table 3
Results of Monte Carlo simulation of global water cycle.

Statistics for all successful realizations:	Mean	($\times 10^{13}$ mol/yr) Mean	Conf.	Min	Max
Ocean island flux		0.52	+0.35 −0.23	0.09	1.2
Mid-ocean ridge flux		0.75	+0.25 −0.24	0.18	1.6
Total arc flux		3.2	+2.3 −1.4	0.17	8.0
Slab-derived arc flux		3.1	+2.3 −1.4	0.13	7.9
Total back-arc flux		0.44	+0.25 −0.28	0.02	0.97
Slab-derived back-arc flux		0.38	+0.26 −0.31	0	0.95
Trench input flux		6.0	+2.6 −1.3	4.1	13
Total mantle-derived output flux = (OIB + MORB + mantle-derived arc + mantle-derived back-arc)		1.4	+0.4 −0.3	0.38	3.0

Net flux and return flux to the mantle[a]:	($\times 10^{13}$ mol/yr) Net flux	Return flux	
Near-steady state scenario:			
0 m over 542 Myr	0	1.4	+0.4 −0.3
100 m over 542 Myr	0.56	2.0	+0.4 −0.3
Maximum permissible sea level change:			
360 m over 542 Myr	2.1	3.5	+0.4 −0.3

[a] Net flux is the difference between mantle return and output fluxes, and is accomodated by a corresponding change in sea level. Statistics for the return flux are calculated based on realizations with a net flux within 10^{11} mol/yr of the net flux for specified sea level change scenarios. Means are given with 68% confidence limits ("conf.").

3. Results

The Monte Carlo approach allows us to quantify the global water fluxes with associated 68% confidence intervals. A simulation of the global water cycle with 10^7 model realizations was performed based on the input parameters given in Table 1. Repeat simulations were performed to ensure that the results had converged. A summary of model results is presented in Table 3. A striking aspect of the simulation is that 86% of the realizations resulted in failure, where one or both of the criteria were violated (Section 2.3). A parameter sensitivity test indicates that arc water output and trench water input exert primary control over the global water cycle, as these two fluxes are significantly larger than the MORB, OIB and back-arc fluxes (Table 3). The total mantle-derived water output flux is $1.4^{+0.4}_{-0.3}\times 10^{13}$ mol/yr (Table 3). The outgassing flux of water at arcs is $3.2^{+2.3}_{-1.4}\times 10^{13}$ mol/yr. While the mean arc output flux is a factor of two higher than the estimate of 1.7×10^{13} mol/yr by Wallace (2005), the two estimates are consistent at the 68% confidence limit.

Fig. 4 shows model success rate contoured across trench water input flux and arc magmatic water content parameter space. Contours indicate the fraction of successful realizations at the specified arc and trench values, given independent random variation in all other parameters, including arc magma production rate. We emphasize that the simulation does not directly provide information about which successful scenarios are most likely to reflect reality—the simulation only determines what regions of parameter space are allowed given the observational constraints. Thus, an area of arc-trench parameter space with low (but non-zero) success rates is not necessarily unrealistic, but it does require very specific tuning of the remaining parameters to satisfy observational constraints.

The most striking aspect of Fig. 4 is that approximately two-thirds of the arc-trench parameter space is devoid of successful realizations. The upper limit trench intake (Schmidt and Poli, 1998) results in zero successful realizations. The highest trench input flux with a success rate > 0.1% is 12×10^{13} mol/yr. The trench input flux estimates of Rüpke et al. (2004), Hacker (2008) and van Keken et al. (2011) result in maximum success rates of ~20, 40, and ~55% at global mean arc H_2O contents of ~6.0, 4.5 and 3.0 wt.%, respectively. Success rate is maximized at low trench inputs and a global mean arc magmatic H_2O of ~2 wt.%: in this region of parameter space, the model is least

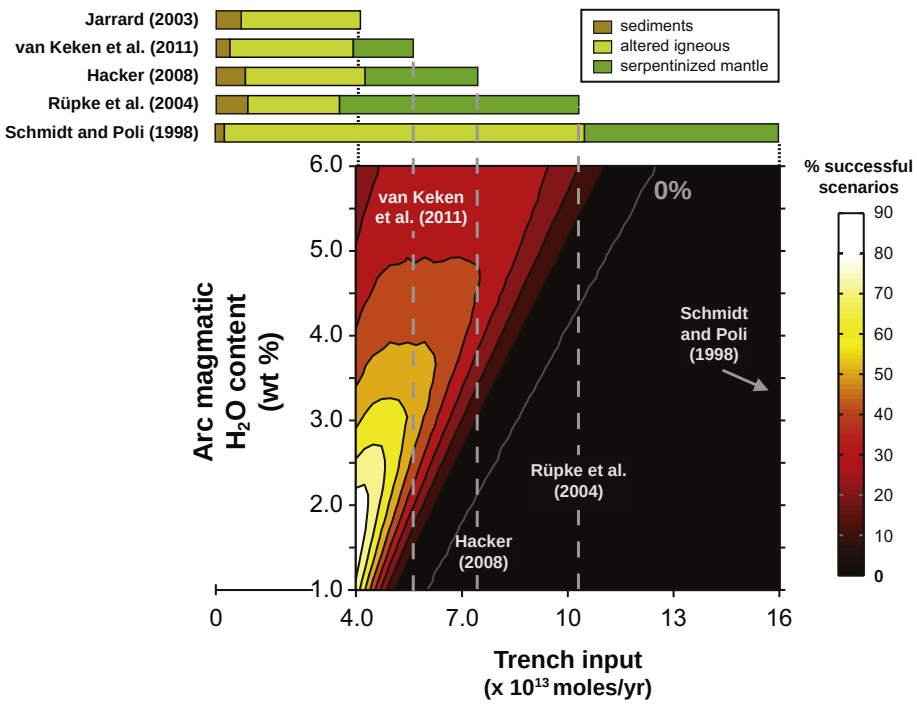

Fig. 4. Contour of model success rate (% successful realizations out of total realizations) as a function of trench H_2O input flux and arc magmatic H_2O content parameter space. Black parameter space is devoid of successful scenarios (100% Failure 2; sea level decrease > 360 m), and makes up ~60% of the arc-trench parameter space explored. The highest trench input flux for which there is a single successful scenario is 12×10^{13} mol per year. Success rate is maximized at low trench inputs and an arc magmatic H_2O content of ~2 wt.%; here, the model is least sensitive to variation in the remaining parameters. Failure 1 occurs only in the upper left corner: here, low trench inputs cannot support the arc fluxes generated given high arc H_2O contents. Failure 2 due to sea level increase > 35 m is also confined to the upper left corner.

sensitive to variations in the remaining parameters. Failure rates increase at high magmatic water contents as the simulation becomes sensitive to arc magma production rate.

To better understand model sensitivity to arc magma production rate, we ran simulations at three magma production rate intervals (Fig. 5): low (1.1–3.5 km^3 per year), medium (3.5–6.0 km^3 per year) and high (6.0–8.6 km^3 per year). At low magma production rates (Fig. 5a), high success rates occur over arc magmatic H_2O contents of 2–5 wt.%, but success is limited to the very lowest trench inputs, and Failure 2 dominates most of the space. Higher arc magma production rates (Fig. 5b, c) enable success at higher trench inputs, but inhibit success at low trench inputs since resulting arc output fluxes are too high to be supported by the trench intake (Failure 1 in the upper left corners of Fig. 5b, c). Fig. 5 also illustrates why maximum model success rate in Fig. 4 occurs near 2 wt.% arc magmatic H_2O and low trench input: this region of parameter space maintains moderate-to-high success rates over all three arc magma production intervals.

4. Discussion

We now explore the implications of our Monte Carlo simulation for water exchange between the mantle and exosphere. We discuss two water cycling scenarios over the past 542 Ma. The first, our preferred scenario based on the available data, is a near steady-state ocean where the return flux of water to the mantle generates between 0 and 100 m of sea level decrease (Section 2.3.2 discusses the evidence supporting this scenario). In the second scenario, the mantle return flux generates the maximum-supported sea level decrease of 360 m over 542 Ma.

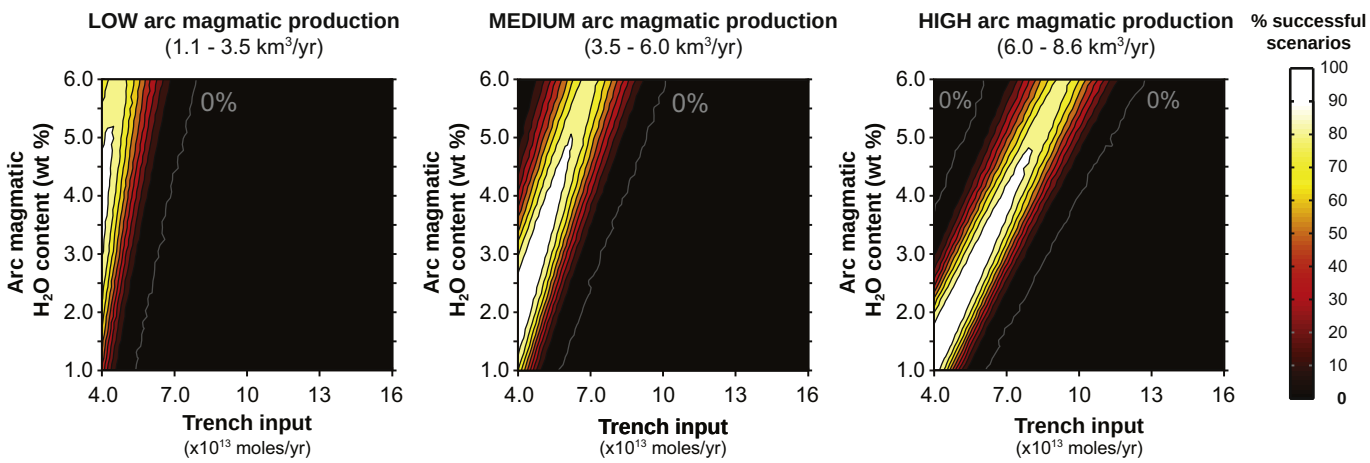

Fig. 5. Contour of model success rate for three different arc magmatic production intervals: (a) a "low" interval (1.1 to 3.5 km^3 per year), (b) an "intermediate" interval (3.5 to 6.0 km^3 per year), and (c) a "high" interval (6.0 to 8.6 km^3 per year). Axes are the same as in Fig. 4.

4.1. The hydration state of subducting slab

Total trench input fluxes are poorly estimated, as illustrated by the large number of failures for most of trench parameter space (Fig. 4). However, estimates of the global trench input flux differ primarily due to varying estimates of the poorly-constrained serpentinized lithospheric mantle water flux; that is, studies agree on the flux of water carried in sediments and altered igneous crust (~4×10^{13} mol/yr, Fig. 4; Jarrard, 2003; Hacker, 2008; Rüpke et al., 2004; van Keken et al., 2011). The trench inputs in realizations that generate our preferred near steady-state ocean (0–100 m sea level decrease) scenario and the maximum sea level scenario are $5.7_{-1.2}-5.9^{+2.2}\times10^{13}$ mol/yr and $6.5^{+2.8}_{-1.4}\times10^{13}$ mol/yr, respectively (means and 68% confidence limits). Assuming that 4.0×10^{13} mol/yr are carried in sediments and altered igneous crust (see above), the trench input flux carried in serpentinized lithospheric mantle ranges from $1.7_{-1.2}-1.9^{+2.2}\times10^{13}$ and $2.5^{+2.8}_{-1.4}\times10^{13}$ mol/yr, corresponding to $2.7_{-1.8}-2.9^{+3.4}$% and $3.8^{+4.3}_{-2.1}$% serpentinization of 10 km of lithospheric mantle, respectively. The preferred near steady-state serpentinite fluxes fall at the low end of estimates given by Schmidt and Poli (1998) and Rüpke et al. (2004), are ~50% lower than estimates by Hacker (2008) and more than 20 times lower than the estimate given by Li and Lee (2006).

We now use the above limits on trench input flux to explore the spatial extent of serpentinization in slabs. Hydration of lithospheric mantle is thought to occur along deep faults formed at the outer rise. We assume a fault spacing of 3 km (Ranero et al., 2003), fault depth of 10 km, and 45,000 km of trench (Jarrard, 2003). If serpentinization reactions begin at fault surfaces and propagate laterally, we calculate a lateral extent of serpentinization of 51–55 m and 73 m from each fault surface (for the near steady-state and 360 m sea level decrease scenarios, respectively; based on pure 13 wt.% H_2O serpentine, 2.6 g/cm^3 density). We note that a laterally continuous serpentinite layer would not form unless the depths of serpentinization were limited to 340–360 m and 480 m, respectively.

4.2. Previous estimates of the return flux of water to the mantle

Previously-estimated return fluxes range from 3.5–9.4×10^{13} (Rüpke et al., 2004), 4.7×10^{13} (Hacker, 2008), and 3.8×10^{13} (van Keken et al., 2011) mol/yr (Fig. 6). Return fluxes are taken as the authors' estimates of bound water flux beyond depths of arc magma generation (~4–5 GPa or 120–150 km; Hacker, 2008; Syracuse and Abers, 2006). Rüpke et al. (2004) provide water release curves with depth; we use these to calculate the range of bound water at 120 km depth (after Hacker, 2008). van Keken et al. (2011) estimate that ~1/3 of their initial slab water input is released above 100 km depth and constitutes the flux supplying global arc volcanism. Another 1/3 of the initial flux is retained beyond 230 km depth and is discussed as the deep mantle return flux. The fate of the remaining 1/3 (released between 100 and 230 km) is unspecified, but since it is largely released below depths of magma generation and the authors do not include it in their arc magmatic flux (van Keken et al., 2011), it is considered here as part of the return flux.

All literature return fluxes exceed the total mantle-derived output flux given by our model (Table 3; Fig. 6), indicating net mantle regassing. Fig. 6 shows the decrease in sea level if the imbalance between the return fluxes and mantle output fluxes are sustained over the entire Phanerozoic. All literature estimates generate sea level change in excess of our preferred limit (0–100 m). Furthermore, most of the estimates also violate the upper limit (360 m) sea level decrease: the estimates of van Keken et al. (2011) and the lower limit of Rüpke et al. (2004) are only compatible with a sea level decrease of 360 m if mantle output is high (Fig. 6). Thus, the vast majority of literature return fluxes are too large to reflect long-term water cycling between the mantle and exosphere. If sustained, they would reduce the amount of exospheric water by an amount inconsistent with reconstructions of Phanerozoic sea level. In particular, the highest estimated return flux (Rüpke et al., 2004) would remove a volume of water equal to half the present-day ocean in 500 Ma.

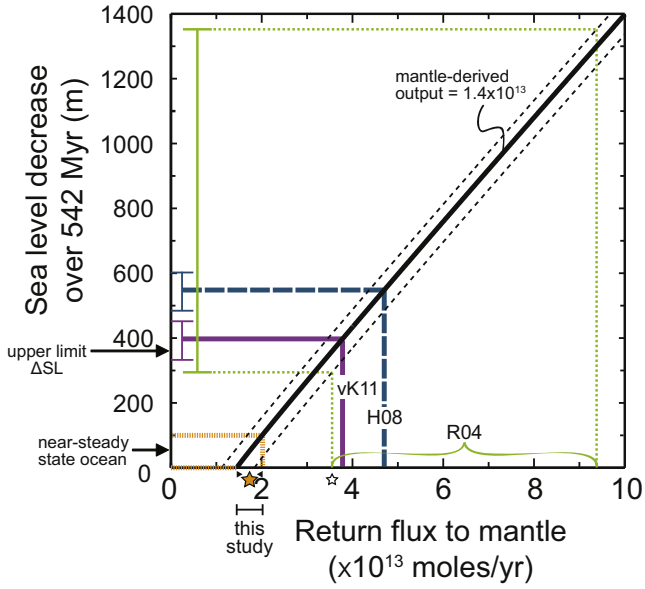

Fig. 6. Sea level decrease over 542 Ma as a function of return flux to the mantle. R04 = Rüpke et al. (2004), H08 = Hacker (2008) and vK11 = van Keken et al. (2011). The solid black line represents sea level change given the mean total mantle-derived output flux of 1.4×10^{13} mol/yr (accompanying dashed black lines represent the 68% confidence limits of total mantle-derived output; 1.1–1.8×10^{13} mol/yr). The range in sea level change for each study is based on the 68% confidence limits of total mantle-derived water output. All literature return flux estimates exceed the near-steady state ocean return flux range. Only at the 68% confidence limit are the estimate of van Keken et al. (2011) and the lower limit of Rüpke et al. (2004) consistent with the upper limit sea level decrease of 360 m. Our preferred return flux based on the near-steady state ocean scenario (0–100 m sea level decrease), is $1.4-2.0^{\pm0.4}_{\pm0.3}\times10^{13}$ mol/yr, indicated by the solid star. Open star indicates our upper limit return flux to the mantle.

4.3. Mantle regassing rates

The sea level reconstructions discussed in Section 2.3.2 indicate that long-term secular decrease in sea level over the Phanerozoic was limited to ~0–100 m. Accordingly, the near steady-state ocean scenario described above yields our preferred return flux range of $1.4-2.0^{\pm0.4}_{\pm0.3}\times10^{13}$ mol/yr to the mantle (Table 3). The upper limit of 360 m of sea level decrease over the Phanerozoic yields a return flux of $3.5^{\pm0.4}_{\pm0.3}\times10^{13}$ mol/yr into the mantle (Table 3). All of these fluxes are low compared to previous estimates (Fig. 6). If the entire return flux is distributed uniformly throughout 10 km of lithospheric mantle as serpentine, the above fluxes correspond to $2.2-3.1^{\pm0.6}_{\pm0.5}$% serpentinization and $5.4^{\pm0.6}_{\pm0.5}$% serpentinization, respectively, assuming 2.7 km^2 of convergence per year and 3.3 g/cm^3 density for lithospheric mantle. These numbers are in some cases higher than the initial serpentinized mantle input fluxes to trenches estimated in Section 4.1, suggesting that up to 70% of the return flux is carried in the igneous crust, in minerals such as lawsonite and phengite (e.g., Hacker, 2008; Schmidt and Poli, 1998; van Keken et al., 2011). It is also possible that all of the previous studies have overestimated the flux of water carried in sediments and altered igneous crust (Fig. 4; Section 4.1), which would allow the initial serpentinized mantle input flux to the trench to be larger.

Our preferred and upper limit return fluxes over the Phanerozoic correspond to preferred and upper limit net mantle regassing rates of 0–5.6×10^{13} mol/yr and of 2.1×10^{13} mol/yr, respectively (Table 3). While we have discussed water cycling only over the Phanerozoic, as observational constraints are strongest for this period of time, we note that the Phanerozoic upper limit of 2.1×10^{13} mol/yr for the net mantle

regassing rate cannot reflect conditions into deep time. Continental freeboard arguments suggest that sea surface height with respect to continents has remained within 500 m of the present value since the end-Archean (Galer, 1991; Kasting and Holm, 1992; Windley, 1977; Wise, 1974), suggesting that the upper limit net flux might only be sustained for up to ~750 Ma; if sustained since the end-Archean, the upper limit would generate ~1600 m of sea level decrease. In contrast, our preferred net regassing flux for the Phanerozoic (0–5.6 × 10^{12} mol/yr) would be consistent into deep time as it would generate a sea level decrease of up to ~0–500 m since 2.5 Ga. The preferred net mantle regassing rate would lead to at most a 60 ppm increase in bulk mantle water content since 2.5 Ga, which is a factor of 3.5 less than van Keken et al.'s (2011) estimate of 200 ppm (370 ppm over 4.5 Ga). However, the factor of 3.5 difference is readily explained by the fact that van Keken et al. (2011) neglect any mantle-derived water output flux in computing the net mantle regassing rate, resulting in an unrealistically high increase in mantle water content.

4.4. Implications for the evolution of mantle volatile budgets

Our preferred and upper limit return fluxes of water to the mantle correspond to bulk water contents in a 100 km-thick slab of 280–400 ppm and 700 ppm H_2O, respectively. Since some part of the return flux may be stored in nominally anhydrous minerals in the mantle wedge without being returned to the exosphere, the bulk slab water contents are upper limits. Convective stirring and assimilation of recycled slabs with our preferred slab water contents of 280–400 ppm into the MORB source could account for the MORB source water, as source concentrations are between 50 and 230 ppm (Saal et al., 2002; Simons et al., 2002). Furthermore, the MORB source may be getting wetter: since water concentrations in the slab are higher than the MORB source, mixing and assimilation should enrich the mantle source. In contrast, convective stirring of recycled slabs is not likely to account for all of the OIB source water (Table 1), particularly for the high $^3He/^4He$ FOZO plumes that have ~750 ppm water in their source (e.g. Dixon et al., 2002). Thus, we suggest that a source of juvenile water is required for OIB magmatism, consistent with the inference of Dixon et al. (2002) based on H_2O/Ce ratios. Furthermore, mixing and assimilation of slabs with 280–400 ppm water may be diluting the OIB source water over time; i.e., the OIB source may be getting drier. It is conceivable that if subducted slabs have the upper limit 700 ppm H_2O, then all of the water in the OIB source could be associated with recycling of subducted water. However, the residence time of material in the OIB source region is on order ~1–2 Ga (Allegre, 2002; Gonnermann and Mukhopadhyay, 2009; Kawabata et al., 2011) and the upper limit slab water content cannot be sustained much further back than 750 Ma.

The relatively low magnitude of our preferred total trench input flux and return flux estimates is significant in light of suggestions that the return flux of water to the mantle affects cycling of other volatiles, such as the noble gases. Since heavy noble gases (e.g., Ar and Xe) have been used to place constraints on mantle structure and dynamics, it is especially important to understand the origin of noble gas signatures. For example, based on apparent similarities in the noble gas abundance patterns of the mantle and seawater, Holland and Ballentine (2006) argue that differences in OIB and MORB source noble gases reflect preferential recycling of seawater-derived atmospheric noble gases into the OIB source. Such a conclusion has important ramifications for mantle geodynamics, as it implies that differences between MORB and OIB noble gases are related to recycling of atmospheric gases, rather than the preservation of a less-degassed mantle source. However, the Holland and Ballentine (2006) hypothesis specifically requires unfractionated atmospheric noble gases dissolved in seawater to be carried as pore water trapped within subducting slabs. Given the difficulty in retaining significant amounts of pore water beyond depths of magma generation, Sumino et al. (2010) propose that the noble gases may be carried by unfractionated seawater trapped in fluid inclusions. To account for the mantle Ar budget, 0.37 × 10^{13} mol/yr of unfractionated seawater trapped within pores or in fluid inclusions must return to the mantle (Holland and Ballentine, 2006). Unless a surprisingly large percentage of the preferred mantle return flux (~20–30%) is carried as pore water or within fluid inclusions, preferential transport of unfractionated noble gases in seawater to the lower mantle to generate the OIB heavy noble gas signature is problematic. We are not aware of any studies that independently document such a large percentage of the return flux to the mantle to be associated with pore water or fluid inclusions. Therefore, a lower degree of degassing for the OIB source remains a viable explanation for differences in MORB and OIB heavy noble gas compositions.

5. Conclusion

We used a Monte Carlo simulation of global water exchange between the mantle and exosphere to constrain the magnitudes of the flux of water (1) into trenches and (2) beyond depths of magma generation, based on reconstructions of Phanerozoic sea level change. We find that previous estimates of both of the above fluxes are frequently too large to reflect long-term water cycling. We estimate trench input fluxes from $5.7_{-1.2} - 5.9^{+2.2} \times 10^{13}$ mol/yr and $6.5^{+2.8}_{-1.4} \times 10^{13}$ mol/yr (near steady-state and upper limit sea level statistics, respectively), which suggest a limited extent of serpentinization of subducting lithospheric mantle. Our preferred return flux to the mantle, based on 0–100 m of sea level decrease over the Phanerozoic, is between $1.4 - 2.0^{+0.4}_{-0.3} \times 10^{13}$ mol/yr. The associated net flux would also be compatible with sea level change since the end-Archean based on continental freeboard, and would lead to an increase in bulk mantle water content of up to 60 ppm since 2.5 Ga. Furthermore, our study indicates that while water in the MORB source may be accounted for by recycling of chemically-bound water in subducted slabs, recycled slab water contents may not be high enough to support all of the OIB source water, such that a juvenile source is required for some fraction of OIB water.

Supplementary materials related to this article can be found online at doi:10.1016/j.epsl.2011.11.024.

Acknowledgments

We thank Jerry Mitrovica and Ved Lekic for discussions, and Rick Carlson for editorial handling. Katherine Kelley and an anonymous reviewer provided comments that helped to improve the manuscript. This work was funded in part by NSF grants OCE 0929193 and EAR 0911363.

References

Abbott, D., Burgess, L., Longhi, J., Smith, W.H.F., 1994. An empirical thermal history of the Earth's upper-mantle. J. Geophys. Res. Solid Earth 99, 13835–13850.

Algeo, T.J., Wilkinson, B.H., 1991. Modern and ancient continental hypsometries. J. Geol. Soc. Lond. 148, 643–653.

Allegre, C.J., 2002. The evolution of mantle mixing. Philos. Trans. R. Soc. A 360, 2411–2431. doi:10.1098/rsta.2002.1075.

Almeev, R., Holtz, F., Koepke, J., Haase, K., Devey, C., 2008. Depths of partial crystallization of H_2O-bearing MORB: phase equilibria simulations of basalts at the MAR near Ascension Island (7–11 degrees s). J. Petrol. 49, 25–45. doi:10.1093/petrology/egm068.

Aubaud, C., Hauri, E.H., Hirschmann, M.M., 2004. Hydrogen partition coefficients between nominally anhydrous minerals and basaltic melts. Geophys. Res. Lett. 31, L20611. doi:10.1029/2004gl021341.

Baker, E.T., German, C.R., 2004. On the global distribution of hydrothermal vent fields. In: German, C.R., Lin, J., Parson, L.M. (Eds.), Mid-ocean Ridges: Hydrothermal Interactions between the Lithosphere and Oceans: AGU Geophysical Monograph Series, 148, pp. 245–266.

Benjamin, E.R., Plank, T., Wade, J.A., Kelley, K.A., Haun, E.H., Alvarado, G.E., 2007. High water contents in basaltic magmas from Irazu volcano, Costa Rica. J. Volcanol. Geotherm. Res. 168, 68–92. doi:10.1016/j.jvolgeores.2007.08.008.

Cervantes, P., Wallace, P.J., 2003. Role of H_2O in subduction-zone magmatism: new insights from melt inclusions in high-Mg basalts from Central Mexico. Geology 31, 235–238.

Conrad, C.P., Husson, L., 2009. Influence of dynamic topography on sea level and its rate of change. Lithosphere 1, 110–120. doi:10.1130/l32.1.

Crisp, J.A., 1984. Rates of magma emplacement and volcanic output. J. Volcanol. Geotherm. Res. 20, 177–211.

Crowley, J.W., Gerault, M., O'Connell, R.J., 2011. On the relative influence of heat and water transport on planetary dynamics. Earth Planet. Sci. Lett. 310, 380–388. doi:10.1016/j.epsl.2011.08.035.

Dixon, J.E., Leist, L., Langmuir, C., Schilling, J.G., 2002. Recycled dehydrated lithosphere observed in plume-influenced mid-ocean-ridge basalt. Nature 420, 385–389. doi:10.1038/nature01215.

Fretzdorff, S., Livermore, R.A., Devey, C.W., Leat, P.T., Stoffers, P., 2002. Petrogenesis of the back-arc East Scotia Ridge, South Atlantic Ocean. J. Petrol. 43, 1435–1467.

Galer, S.J.G., 1991. Inter-relationships between continental freeboard, tectonics and mantle temperature. Earth Planet. Sci. Lett. 105, 214–228.

Gonnermann, H.M., Mukhopadhyay, S., 2009. Preserving noble gases in a convecting mantle. Nature 459, 560–U588. doi:10.1038/Nature08018.

Hacker, B.R., 2008. H_2O subduction beyond arcs. Geochem. Geophys. Geosyst. 9, Q03001. doi:10.1029/2007gc001707.

Hallam, A., 1984. Pre-Quaternary sea-level changes. Annu. Rev. Earth Planet. Sci. 12, 205–243.

Hallam, A., 1992. Phanerozoic Sea Level Changes. Columbia University Press, New York. 266 pp.

Haq, B.U., Schutter, S.R., 2008. A chronology of Paleozoic sea-level changes. Science 322, 64–68. doi:10.1126/science.1161648.

Haq, B.U., Hardenbol, J., Vail, P.R., 1987. Chronology of fluctuating sea levels since the Triassic. Science 235, 1156–1167.

Hardenbol, J.R., Vail, P.R., Ferrer, J., 1981. Interpreting paleoenvironments, subsidence history and sea-level changes of passive margins from seismic and biostratigraphy. Proceedings 26th International Geological Congress, Geology of Continental Margins Symposium, Paris, 7–17 July, 1980 Supplement to Volume: Oceanologica Acta, 3, pp. 33–44.

Harrison, C.G.A., 1990. Long-term eustasy and epeirogeny in continents. In: N. R. C. Geophysics Study Committee (Ed.), Sea-level Change. National Academy Press, Washington, D. C., pp. 141–158.

Hauri, E.H., Gaetani, G.A., Green, T.H., 2006. Partitioning of water during melting of the Earth's upper mantle at H_2O-undersaturated conditions. Earth Planet. Sci. Lett. 248, 715–734. doi:10.1016/j.epsl.2006.06.014.

Hays, J.D., Pitman, W.C., 1973. Lithospheric plate motion, sea-level changes and climatic and ecological consequences. Nature 246, 18–22.

Hirschmann, M.M., 2006. Water, melting, and the deep Earth H_2O cycle. Annu. Rev. Earth Planet. Sci. 34, 629–653. doi:10.1146/annurev.earth.34.031405.125211.

Hirth, G., Kohlstedt, D.L., 1996. Water in the oceanic upper mantle: Implications for rheology, melt extraction and the evolution of the lithosphere. Earth Planet. Sci. Lett. 144, 93–108.

Holland, G., Ballentine, C.J., 2006. Seawater subduction controls the heavy noble gas composition of the mantle. Nature 441, 186–191. doi:10.1038/Nature04761.

Inoue, T., 1994. Effect of water on melting phase-relations and melt composition in the system Mg_2SiO_4–$MgSiO_3$–H_2O up to 15 GPa. Phys. Earth Planet. Inter. 85, 237–263.

Jarrard, R.D., 2003. Subduction fluxes of water, carbon dioxide, chlorine, and potassium. Geochem. Geophys. Geosyst. 4, 8905. doi:10.1029/2002gc000392.

Johnson, E.R., Wallace, P.J., Granados, H.D., Manea, V.C., Kent, A.J.R., Bindeman, I.N., Donegan, C.S., 2009. Subduction-related volatile recycling and magma generation beneath Central Mexico: insights from melt inclusions, oxygen isotopes and geodynamic models. J. Petrol. 50, 1729–1764. doi:10.1093/petrology/egp051.

Karato, S.I., Jung, H., 2003. Effects of pressure on high-temperature dislocation creep in olivine. Philos. Mag. 83, 401–414. doi:10.1080/0141861021000025829.

Kasting, J.F., Holm, N.G., 1992. What determines the volume of the oceans? Earth Planet. Sci. Lett. 109, 507–515.

Kawabata, H., Hanyu, T., Chang, Q., Kimura, J.I., Nichols, A.R.L., Tatsumi, Y., 2011. The petrology and geochemistry of St. Helena alkali basalts: evaluation of the oceanic crust-recycling model for HIMU OIB. J. Petrol. 52, 791–838. doi:10.1093/petrology/egr003.

Kelley, K.A., Plank, T., Grove, T.L., Stolper, E.M., Newman, S., Hauri, E., 2006. Mantle melting as a function of water content beneath back-arc basins. J. Geophys. Res. Solid Earth 111, B09208. doi:10.1029/2005jb003732.

Kelley, K.A., Plank, T., Newman, S., Stolper, E.M., Grove, T.L., Parman, S., Hauri, E.H., 2010. Mantle melting as a function of water content beneath the Mariana Arc. J. Petrol. 51, 1711–1738. doi:10.1093/petrology/egq036.

Labrosse, S., Jaupart, C., 2007. Thermal evolution of the Earth: secular changes and fluctuations of plate characteristics. Earth Planet. Sci. Lett. 260, 465–481. doi:10.1016/j.epsl.2007.05.046.

Langmuir, C.H., Bezos, A., Escrig, S., Parman, S.W., 2006. Chemical systematics and hydrous melting of the mantle in back-arc basins. In: Christie, D.M., Fisher, C.R., Lee, S.-M., Givens, S. (Eds.), Back-arc Spreading Systems: Geological, Biological, Chemical, and Physical Interactions: AGU Geophysical Monograph Series, 166, pp. 87–146.

Lee, C.T.A., Leeman, W.P., Canil, D., Li, Z.X.A., 2005. Similar V/Sc systematics in MORB and arc basalts: implications for the oxygen fugacities of their mantle source regions. J. Petrol. 46, 2313–2336. doi:10.1093/petrology/egi056.

Li, Z.X.A., Lee, C.T.A., 2006. Geochemical investigation of serpentinized oceanic lithospheric mantle in the Feather River Ophiolite, California: implications for the recycling rate of water by subduction. Chem. Geol. 235, 161–185. doi:10.1016/j.chemgeo.2006.06.011.

Mei, S., Kohlstedt, D.L., 2000. Influence of water on plastic deformation of olivine aggregates 2. Dislocation creep regime. J. Geophys. Res. Solid Earth 105, 21471–21481.

Michael, P., 1995. Regionally distinctive sources of depleted MORB — evidence from trace-elements and H_2O. Earth Planet. Sci. Lett. 131, 301–320.

Miller, K.G., Wright, J.D., Fairbanks, R.G., 1991. Unlocking the ice house — Oligocene–Miocene oxygen isotopes, eustasy, and margin erosion. J. Geophys. Res. Solid 96, 6829–6848.

Miller, K.G., Kominz, M.A., Browning, J.V., Wright, J.D., Mountain, G.S., Katz, M.E., Sugarman, P.J., Cramer, B.S., Christie-Blick, N., Pekar, S.F., 2005. The Phanerozoic record of global sea-level change. Science 310, 1293–1298. doi:10.1126/science.1116412.

Moucha, R., Forte, A.M., Mitrovica, J.X., Rowley, D.B., Quere, S., Simmons, N.A., Grand, S.P., 2008. Dynamic topography and long-term sea-level variations: there is no such thing as a stable continental platform. Earth Planet. Sci. Lett. 271, 101–108. doi:10.1016/j.epsl.2008.03.056.

Muller, R.D., Sdrolias, M., Gaina, C., Steinberger, B., Heine, C., 2008. Long-term sea-level fluctuations driven by ocean basin dynamics. Science 319, 1357–1362. doi:10.1126/science.1151540.

Nedimovic, M.R., Bohnenstiehl, D.R., Carbotte, S.M., Canales, J.P., Dziak, R.P., 2009. Faulting and hydration of the Juan de Fuca plate system. Earth Planet. Sci. Lett. 284, 94–102. doi:10.1016/j.epsl.2009.04.013.

Newman, S., Stolper, E., Stern, R., 2000. H_2O and CO_2 in magmas from the Mariana arc and back-arc systems Geochem. Geophys. Geosyst. 1, 1013. doi:10.1029/1999GC000027.

Parsons, B., 1982. Causes and consequences of the relation between area and age of the ocean-floor. J. Geophys. Res. 87, 289–302.

Pineau, F., Shilobreeva, S., Hekinian, R., Bideau, D., Javoy, M., 2004. Deep-sea explosive activity on the Mid-Atlantic Ridge near 34°50′N: A stable isotope (C, H, O) study. Chem. Geol. 211, 159–175. doi:10.1016/j.chemgeo.2004.06.029.

Plank, T., 2005. Constraints from thorium/lanthanum on sediment recycling at subduction zones and the evolution of the continents. J. Petrol. 46, 921–944. doi:10.1093/petrology/egi005.

Portnyagin, M., Hoernle, K., Plechov, P., Mironov, N., Khubunaya, S., 2007. Constraints on mantle melting and composition and nature of slab components in volcanic arcs from volatiles (H_2O, S, Cl, F) and trace elements in melt inclusions from the Kamchatka Arc. Earth Planet. Sci. Lett. 255, 53–69.

Ranero, C.R., Morgan, J.P., Mcintosh, K., Reichert, C., 2003. Bending-related faulting and mantle serpentinization at the Middle America trench. Nature 425, 367–373. doi:10.1038/Nature01961.

Ranero, C.R., Villasenor, A., Phipps-Morgan, J., Weinrebe, W., 2005. Relationship between bend-faulting at trenches and intermediate-depth seismicity. Geochem. Geophys. Geosyst. 6, Q12002. doi:10.1029/2005gc000997.

Reymer, A., Schubert, G., 1984. Phanerozoic addition rates to the continental-crust and crustal growth. Tectonics 3, 63–77.

Roggensack, K., 2001. Sizing up crystals and their melt inclusions: a new approach to crystallization studies. Earth Planet. Sci. Lett. 187, 221–237.

Rowley, D.B., 2002. Rate of plate creation and destruction: 180 Ma to present. Geol. Soc. Am. Bull. 114, 927–933.

Rüpke, L.H., Morgan, J.P., Hort, M., Connolly, J.A.D., 2004. Serpentine and the subduction zone water cycle. Earth Planet. Sci. Lett. 223, 17–34.

Ruscitto, D.M., Wallace, P.J., Johnson, E.R., Kent, A.J.R., Bindeman, I.N., 2010. Volatile contents of mafic magmas from cinder cones in the Central Oregon High Cascades: implications for magma formation and mantle conditions in a hot arc. Earth Planet. Sci. Lett. 298, 153–161. doi:10.1016/j.epsl.2010.07.037.

Ryerson, F.J., Watson, E.B., 1987. Rutile saturation in magmas: implications for Ti–Nb–Ta depletion in island-arc basalts. Earth Planet. Sci. Lett. 86, 225–239.

Saal, A.E., Hauri, E.H., Langmuir, C.H., Perfit, M.R., 2002. Vapour undersaturation in primitive mid-ocean-ridge basalt and the volatile content of Earth's upper mantle. Nature 419, 451–455.

Sadofsky, S.J., Portnyagin, M., Hoernle, K., Van Den Bogaard, P., 2008. Subduction cycling of volatiles and trace elements through the Central American Volcanic Arc: evidence from melt inclusions. Contrib. Mineral. Petrol. 155, 433–456. doi:10.1007/s00410-007-0251-3.

Schmidt, M.W., Poli, S., 1998. Experimentally based water budgets for dehydrating slabs and consequences for arc magma generation. Earth Planet. Sci. Lett. 163, 361–379.

Schmidt, M.W., Poli, S., 2003. 3.17 - Generation of mobile components during subduction of oceanic crust. In: Heinrich, D.H., Turekian, K.K. (Eds.), Treatise on Geochemistry, Vol. 3. Pergamon, Oxford, pp. 567–591.

Schubert, G., Reymer, A.P.S., 1985. Continental volume and freeboard through geological time. Nature 316, 336–339.

Shaw, A.M., Hauri, E.H., Fischer, T.P., Hilton, D.R., Kelley, K.A., 2008. Hydrogen isotopes in Mariana Arc melt inclusions: implications for subduction dehydration and the deep-Earth water cycle. Earth Planet. Sci. Lett. 275, 138–145. doi:10.1016/j.epsl.2008.08.015.

Simons, K., Dixon, J., Schilling, J.G., Kingsley, R., Poreda, R., 2002. Volatiles in basaltic glasses from the Easter-Salas y Gomez seamount chain and Easter microplate: implications for geochemical cycling of volatile elements. Geochem. Geophys. Geosyst. 3, 1039. doi:10.1029/2001gc000173.

Sisson, T.W., Bronto, S., 1998. Evidence for pressure-release melting beneath magmatic arcs from basalt at Galunggung, Indonesia. Nature 391, 883–886.

Standish, J.J., Dick, H.J.B., Michael, P.J., Melson, W.G., O'hearn, T., 2008. MORB generation beneath the ultraslow spreading Southwest Indian ridge (9–25°E): major element chemistry and the importance of process versus source. Geochem. Geophys. Geosyst. 9, Q05004. doi:10.1029/2008gc001959.

Stolper, E., Newman, S., 1994. The role of water in the petrogenesis of Mariana trough magmas. Earth Planet. Sci. Lett. 121, 293–325.

Sumino, H., Burgess, R., Mizukami, T., Wallis, S.R., Holland, G., Ballentine, C.J., 2010. Seawater-derived noble gases and halogens preserved in exhumed mantle wedge peridotite. Earth Planet. Sci. Lett. 294, 163–172. doi:10.1016/j.epsl.2010.03.029.

Syracuse, E.M., Abers, G.A., 2006. Global compilation of variations in slab depth beneath arc volcanoes and implications. Geochem. Geophys. Geosyst. 7, Q05017. doi:10.1029/2005gc001045.

Vail, P.R., Mitchum, R.M., Thompson, S., 1977. Seismic stratigraphy and global changes of sea level, Part 4: global cycles of relative changes of sea level. In:

Clayton, C.E. (Ed.), Seismic Stratigraphy — Applications to Hydrocarbon Exploration. Tulsa, Oklahoma: American Association of Petroleum Geologists Memoir, 26, pp. 83–98.

van Keken, P.E., Ballentine, C.J., Porcelli, D., 2001. A dynamical investigation of the heat and helium imbalance. Earth Planet. Sci. Lett. 188, 421–434.

van Keken, P.E., Hacker, B.R., Syracuse, E.M., Abers, G.A., 2011. Subduction factory: 4. Depth-dependent flux of H_2O from subducting slabs worldwide. J. Geophys. Res. Solid Earth 116, B01401. doi:10.1029/2010jb007922.

Vlaar, N.J., Vankeken, P.E., Vandenberg, A.P., 1994. Cooling of the Earth in the Archean — consequences of pressure-release melting in a hotter mantle. Earth Planet. Sci. Lett. 121, 1–18.

Walker, J.A., Roggensack, K., Patino, L.C., Cameron, B.I., Matias, O., 2003. The water and trace element contents of melt inclusions across an active subduction zone. Contrib. Mineral. Petrol. 146, 62–77. doi:10.1007/s00410-003-0482-x.

Wallace, P.J., 2005. Volatiles in subduction zone magmas: concentrations and fluxes based on melt inclusion and volcanic gas data. J. Volcanol. Geotherm. Res. 140, 217–240. doi:10.1016/j.jvolgeores.2004.07.023.

Windley, B.F., 1977. Timing of continental growth and emergence. Nature 270, 426–428.

Wise, D.U., 1974. Continental margins, freeboard and volumes of continents and oceans through time. In: Nairn, A.E.M., Stehli, F.G. (Eds.), The Geology of Continental Margins. Springer, New York, pp. 45–58.

Xu, X.Q., Lithgow-Bertelloni, C., Conrad, C.P., 2006. Global reconstructions of Cenozoic seafloor ages: implications for bathymetry and sea level. Earth Planet. Sci. Lett. 243, 552–564. doi:10.1016/j.epsl.2006.01.010.

Zachos, J., Pagani, M., Sloan, L., Thomas, E., Billups, K., 2001. Trends, rhythms, and aberrations in global climate 65 Ma to present. Science 292, 686–693.

Zimmer, M.M., Plank, T., Hauri, E.H., Yogodzinski, G.M., Stelling, P., Larsen, J., Singer, B., Jicha, B., Mandeville, C., Nye, C.J., 2010. The role of water in generating the calc-alkaline trend: new volatile data for Aleutian magmas and a new tholeiitic index. J. Petrol. 51, 2411–2444. doi:10.1093/petrology/egq062.